Model Validation and Controller Design for Vibration Suppression of Flexible Rotor Using AMB

Soo Jeon

Graduate Student, Department of Mechanical Engineering, University of California at Berkeley, CA 94720, USA

Hyeong-Joon Ahn

Research Associate, Institute of Advanced Machinery and Design, Seoul National University, Seoul 151-745, Korea

Dong-Chul Han*

Professor, School of Mechanical & Aerospace Engineering, Seoul National University, Seoul 151-745, Korea

This paper discusses the model validation and vibration suppression of an AMB flexible rotor via additional LQG controller. The main difficulty in the vibration suppression of the flexible rotor using AMB is to realize a controller that can minimize resonance without injuring the stabilized rigid modes. In order to solve this problem, simple scheme for system modeling and controller design are developed. Firstly, the AMB flexible rotor is stabilized with a PID controller, which leads to a new stable rotor-bearing system. Then, authors propose the model validation procedure using measured open-loop frequency responses to obtain an accurate model of the AMB flexible rotor system. After that, LQG controller with modal weighting is designed to suppress resonances of the stable rotor-bearing system. Due to the poor controllability and observability of flexible modes compared to rigid ones, balancing of two Gramians is prerequisite for the fair LQG controller design. Simulation with step disturbance and experimental results of unbalance response up to 10,000 rpm verified the effectiveness of the proposed scheme.

Key Words : Active Magnetic Bearing, Flexible Rotor, Vibration Suppression, LQG Control

Nomenclature

C : System damping matrix
D : Diagonal matrix related to modal damping
f : Force vector
$G(j\omega)$: Open-loop FRF measurement data
$G(\omega)$: Gyroscopic matrix
$G(s)$: Transfer function matrix
i : Current

* Corresponding Author,
 E-mail : dchan@amed.snu.ac.kr
 TEL : +82-2-880-7139; **FAX** : +82-2-883-1513
 Professor School of Mechanical & Aerospace Engineering, Seoul National University, Seoul 151-745, Korea. (Manuscript **Received** December 5, 2001; **Revised** September 12, 2002)

J_{LQ} : Performance index of LQ regulator
K : System stiffness matrix
K_i : Current gain matrix of AMB
k_i : Current gain of AMB
K_x : Open-loop stiffness matrix of AMB
k_s : Open-loop stiffness of AMB
m : Shaft mass
m_k : Effective mass of flexible mode
m_r : Effective mass of rigid mode
q : Displacement at each node of shaft element
q_i : Sub-blocks of modal state weighting matrix
Q_{mod} : State weighting matrix of modal system
R : Input weighting matrix
R_r, R_f : Residual matrices

T_{bal} : Transformation matrix from modal state to balanced state

u : General input

$U(jw)$: Open-loop FRF measurement input data

x : Modal state vector

y : Output vector

$Y(j\omega)$: Open-loop FRF measurement output data

Φ : Generalized right eigenvector matrix

Ω : Diagonal matrix related to the square of natural frequency

χ : Balanced state vector

ω : Frequency

ω_n : n^{th} natural frequency

ξ : Modal coordinate vector

ζ : Modal damping factor

Subscripts

r : Rigid body mode

f : Flexible mode

1. Introduction

The vibration problems in flexible rotor-bearing systems have been gaining interest in turbo machinery industry. It is essential to guarantee smooth and efficient running in such rotor bearing systems because large vibration amplitude of a rotor may cause severe damages and even failure of the whole system. Moreover, vibration problem becomes more severe since recent manufacturers are likely to increase the operating speed. The conventional elements such as passive damper were inefficient in that they are additional elements other than bearings and cannot cope with several critical speeds at the same time.

Active magnetic bearings (AMB) can adjust dynamic characteristic of bearing and suppress the vibration through active control. Many works during the last few decades made it clear the great applicability of AMB as both bearing element and vibration suppressor (Schweitzer et al., 1994 ; Lee and Kim, 1992). Since Nonami (Nonami, 1985) and Salm (Salm, 1988) considered the complete active suspension of an AMB flexible rotor, many researchers have investigated the charac-

teristics of AMB flexible rotor systems and suggested various control schemes for both stable levitation and vibration suppression. Okada et al. (Okada et al., 1997) used locally parameterized modal PD controller with the addition of H∞ controller in order to minimize the resonance and to overcome spillover effects.

AMB flexible rotor has difficulties in a stable operation compared to AMB rigid rotor, since they contain lightly damped flexible modes as well as unstable rigid modes. The main objective of this paper is therefore to realize a controller that can suppress resonance peak effectively without injuring the stabilized rigid modes. Recently, Nonami and Ito (Nonami and Ito, 1994), Schonhoff et al. (Schonhoff et al., 2000) and some other researchers have been trying to find a solution of this problem via recently developed μ synthesis. However, satisfactory results in AMB flexible rotor have not been found yet.

In addition, the equation of magnetic force is intrinsically nonlinear and the approximate linear model near an operating point is mostly used to control an AMB system. So far, the identifications of AMB systems have been performed to get the experimental values of physical parameters accurately, which were usually the current gain and open-loop stiffness of AMB or open-loop system poles (Ha and Lee, 1997 ; Kim and Lee, 1998). Although the identification of the parameters is important, validation of augmented whole system is needed with measured overall open-loop frequency responses including all time delay components such as sensor, power amplifier and discretization dynamics.

This paper discusses the model validation and vibration suppression of AMB flexible rotor via additional LQG controller. Firstly, theoretical rotor model is obtained with FEM and is corrected through impulse test. The AMB flexible rotor is stabilized with a PID controller, which leads to a new stable rotor-bearing system. The whole system model is validated by measuring the open-loop frequency responses including AMB and time delay components. An additional LQG controller with modal weighting is designed to suppress the resonances. Simulation with step

disturbance and experimental results of unbalance response up to 10,000 rpm verified the effectiveness of the proposed scheme.

2. Modeling

2.1 Modal analysis

The system used in this work is composed of one mid-span disc for unbalance mass, two AMB rotors, and a flexible coupling as shown in Fig. 1. Two AMB rotors are assembled with power lock, which gives us a similar effect of interference fit with axial bolting.

A general representation of the flexible rotor system using finite element method results in the standard equation of motion as follows

$$M\ddot{q} + (C + G(\omega))\dot{q} + Kq = f \tag{1}$$

where M, C, $G(\omega)$ and K denote mass, damping, gyroscopic and stiffness matrices, and q and f represent displacement and external force vector, respectively. External force term related to AMB can be expressed with linearized electromagnetic force equation as Eq. (2).

$$f = K_x q + K_i i \tag{2}$$

where K_x and K_i indicate open-loop stiffness matrix and current gain matrix of AMB, respectively. Although the magnetic force equation is nonlinear over the full operation range, the mathematical model can be approximated as the linear one near an operating point and this linear model is used in most AMB applications. While the force-current relationship is linear near the operating point, the force displacement relationship doesn't show good linearity and the open-loop stiffness K_x is quite sensitive to small

variations in operating point. The problem is that the open-loop stiffness is the key parameter that governs the unstable real poles of AMB system. Therefore, identification of AMB systems typically has focused on obtaining accurate values of the current gain and open-loop stiffness.

If we neglect frequency dependent gyroscopic effect considering the relatively small operation range, i.e. below 10,000 rpm, we can decouple the whole system into two decoupled systems with two inputs and two outputs. Accordingly, Eq. (1) can be transformed into the modal coordinate of Eq. (3), and corresponding state-space representation of the decoupled system is given by Eq. (4).

$$\ddot{\xi} + 2\zeta\omega\dot{\xi} + \omega^2\xi = \Phi^{-1}K_i i \tag{3}$$

$$\dot{x} = \begin{bmatrix} 0 & I \\ -\Omega & D \end{bmatrix} x + \begin{bmatrix} 0 \\ \Phi^{-1}K_i \end{bmatrix} i \tag{4}$$

$$y = [\Phi \quad 0] x$$

where $x[\xi \quad \dot{\xi}]^T$, Φ denotes the generalized right eigenvector matrix of $K-K_x$, $M\Omega = diag$ $(| -\omega_{r1}^2 \quad -\omega_{r2}^2 \quad \omega_{f1}^2 \cdots \omega_{fn}^2 |)$, and $D = 2 \cdot diag$ $(| \zeta_{r1}\omega_{r1} \quad \zeta_{r2}\omega_{r2} \quad \zeta_{f1}\omega_{f1} \cdots \zeta_{fn}\omega_{fn} |)$.

The state-space representation of Eq. (4) constructs the transfer function matrix $G(s) = C(sI-A)^{-1}B$ of which each element can be rewritten as a sum of second order systems:

$$G(s) = \sum_{j=1}^{2} \frac{R_{rj}}{(s^2 + 2\zeta_{rj}\omega_{rj}s - \omega_{rj}^2)} + \sum_{j=1}^{n} \frac{R_{fj}}{(s^2 + 2\zeta_{fj}\omega_{fj}s + \omega_{fj}^2)} \tag{5}$$

The first term indicates unstable rigid modes, and the second term represents lightly damped flexible modes. The pole-zero configuration of this transfer function is given in Fig. 2. The four
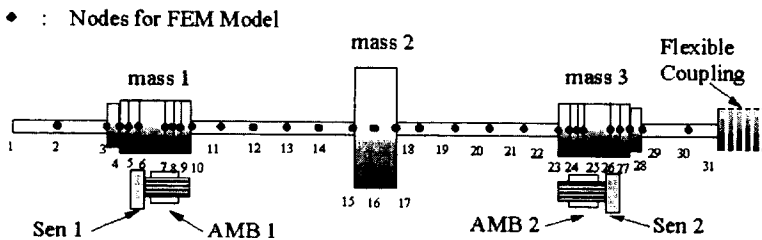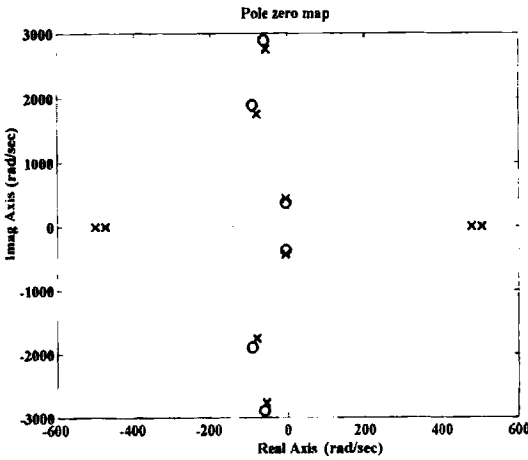

Fig. 1 Schematic of the rotor-bearing system

Fig. 2　Pole-zero configuration

Table 1　Natural frequencies of impulse test and FEM model

	Impulse Test (Hz)	FEM (Hz)
1^{sh}	75	73
2nd	251	247
3rd	376	372
4th	611	621

Fig. 3　Impulse response of the rotor

real poles indicate the two rigid modes while complex poles represent lightly damped bending modes. In case of an AMB rigid rotor, complex poles are very far from real axis compared to real poles and their effects can be negligible in the low frequency range where the real poles are dominant. Therefore, the real and complex poles of the AMB rigid rotor can be identified separately in low and high frequency range, respectively (Ahn, 2001). However, in case of an AMB flexible rotor, the effects of real and complex poles cannot be separated and it is very difficult to identify an AMB flexible rotor system (Gahler and Mohler, 1996).

In this work, commercial FEM package *RO-DAP* (D&M, 2000) is used to construct the state space model of the rotor, and ten modes (two rigid and eight flexible modes) are considered.

2.2　Experimental impulse test

In order to match FEM model with the actual rotor, impulse test is performed. Totally eleven nodal points are selected considering the sensor and bearing locations. The frequency responses are measured with HP dynamic analyzer 35670A, Kistler impulse hammer 9904A, and accelerometer 8462A. The appropriate collection of impulse test results in a 3D plot as shown in Fig. 3, which gives the insight of the modal characteristic of the flexible rotor. The 3D plot of FRF up to 800 Hz, approximately above 4th bending mode, is illu-
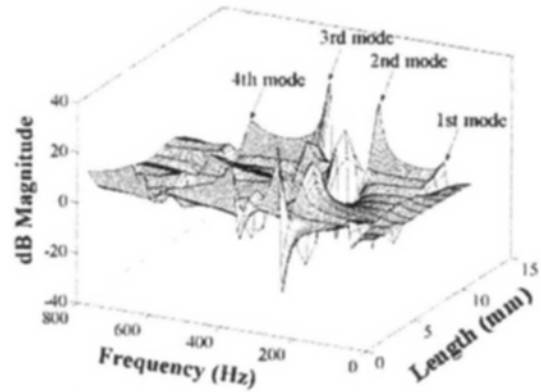
strated in Fig. 3. The result of the impulse test is mainly used to determine the effective bending diameter at locations of the AMB rotors. Comparisons between resulting natural frequencies of FEM model and impulse test are given in Table 1.

2.3　Model validation with open-loop FRF measurement

Firstly, the AMB flexible rotor is stabilized with a PID controller, which leads to a new stable rotor-bearing system. Then, open-loop frequency response functions of the stable rotor bearing system are measured with following procedure.

The closed-loop response vectors u and y due to the excitation f are measured to estimate the non-parametric frequency response function (FRF) of the open-loop plant. The frequency spectra vectors of input and output signals are $U^{(i)}(J\omega) \in C^{nu \times 1}$, $Y^{(i)}(J\omega) \in C^{ny \times 1}$, $i = 1, 2, \cdots,$ N_{exp}. Here, nu, ny is the number of inputs and outputs, and N_{exp} is the number of experiments, respectively. Defining the input/output data matrices at the frequency ω as

$$Y(j\omega) = [\, Y^{(1)}(j\omega)\ Y^{(2)}(j\omega) \cdots Y^{(Nexp)}(j\omega)\,]^T \tag{6}$$
$$\in C^{ny \times Nexp}$$

$$U(j\omega) = [\, U^{(1)}(j\omega)\ U^{(2)}(j\omega) \cdots U^{(Nexp)}(j\omega)\,]^T \tag{7}$$
$$\in C^{nu \times Nexp}$$

Then non-parametric transfer function matrix of open-loop plant $G(J\omega) \in C^{ny \times nu}$ can be obtained by following equation (Pintelon et al., 1998).

$$G(j\omega) = Y(j\omega)\ U(j\omega)^+ \tag{8}$$

Here superscript $+$ denotes the Moore-Penrose pseudo-inverse.

The 11,000 data with 10 kHz sampling frequency are captured to calculate the FFT of input and output signals. Data of initial 0.2 sec (2,000 data) is discarded in order to exclude the transient vibration and time delay of 0.4 sec (4,000 data) between each excitation is introduced to reduce the effect of the previous excitation. Four control inputs and four actuator outputs are measured in one excitation frequency. Also sinusoidal excitations are applied to the system four times at each frequency starting from 0.9 to 721 Hz by about 0.9 Hz step, which corresponds to 800 frequency points.

The measured open-loop FRF of the system are shown in Fig. 5. Each row represents the position of each sensor where the output is measured, and each column corresponds to the position of each magnetic actuator where the excitation signal is applied. Note that 2×2 FRF is not symmetric on its diagonal because of non-collocation of sensor and actuator. There are several mismatches between theoretical and measured FRF including DC gain, roll-off rate, phase lag and modal parameters of flexible poles. In addition, since the frequency spectra vectors of
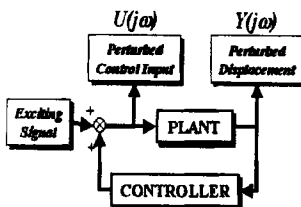
input and output signals are measured in the digital controller, the several time delay components including zero order hold, computational time delay, sensor and actuator dynamics are included in the estimated plant. Therefore, there is a big phase difference between measured and theoretical FRF due to time delay components as shown in Fig. 5. The advantage of including the time delay components is that the non-minimum phase nature of delayed plant manifests itself at controller design stage so that the resulting digital controller compensates for the time delay components. However, there are fundamental limitations in achievable control performance of the non-minimum phase plant. (Lewis, 1992)

The open-loop stiffness k_x is related to the roll off rate of open-loop FRF and the current gain k_i contributes to the DC gain. Usually, k_x and k_i
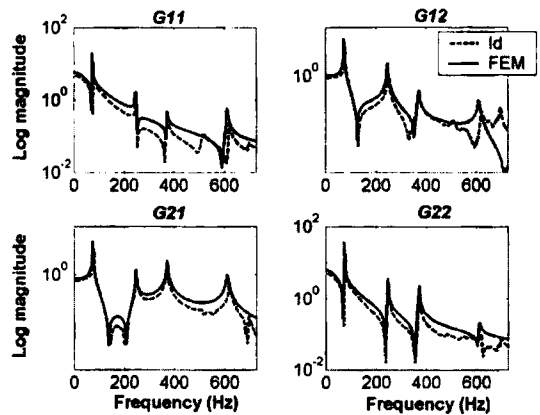
(a) Magnitude
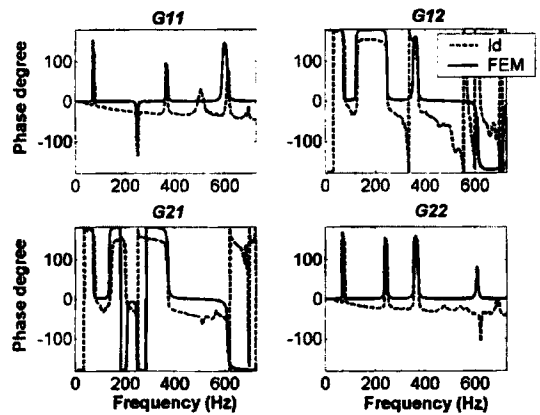
(b) Phase

Fig. 5 Measured and theoretical open-loop FRF

Fig. 4 System block diagram for open-loop plant FRF]

contribute to the most dominant modeling error in AMB systems since they are inversely proportional to the cubic and square of the nominal gap, respectively. A small variation of the nominal gap or operating point, therefore, could result in considerable changes of open-loop stiffness and current gain. The phase lag of the open-loop
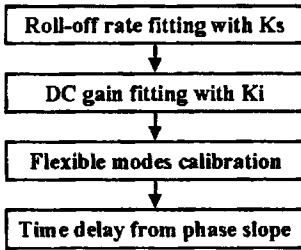
Fig. 6   General procedure for model validation

(a) Magnitude

(b) Phase

Fig. 7   Measured and corrected open-loop FRF

FRF results from several time delay components, as mentioned before. Based on this information, reasonable model validation procedure is shown in Fig. 6. Measured and validated FRFs are shown in Fig. 7 and two FRFs match very well.
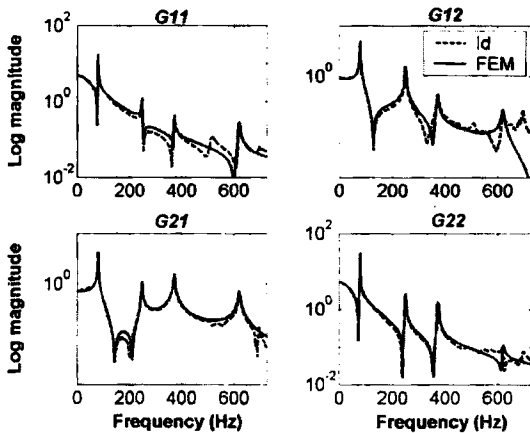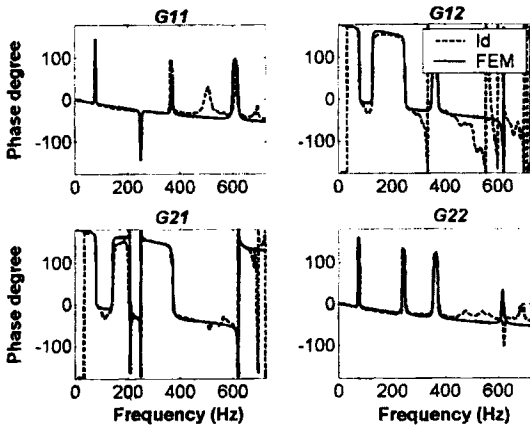
3. Controller Design

A parallel control scheme for the plant stabilized with a PID control is designed in this work instead of complete controller. Figure 8 shows the block diagram of the overall system including the additional LQG controller. The LQG control design method is adopted as parallel controller since LQG can easily adjust system performance through selecting appropriate weighting function. The direct implementation of a LQG control for the original unstable model is very difficult for two reasons. Firstly, LQG control scheme is very sensitive to the modeling error, since there is no guaranteed stability margin in LQG control. Secondly, the weighting of flexible modes directly affects the unstable rigid modes and it is hard to achieve the desired performance of vibration suppression. The stabilization with a PID control renders the model qualification for LQG control scheme, since an accurate model of the flexible rotor was obtained in the previous stage.

The plant stabilized with a PID control shows the typical behavior of the rotor that is supported by normal bearings, since an AMB with a PD controller has the same characteristics as a normal bearing modeled by stiffness and damping coefficient. Figure 9 illustrates the Campbell diagram of the stabilized plant. Two asymptotes of critical speeds considering the gyroscopic effect
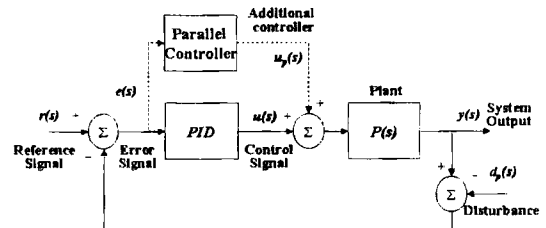
Fig. 8   System block diagram for vibration control

Table 2   Parameters for LQG control

LQ parameters		Kalman estimator parameters	
State weighting Q_k	$Q_k = diag(q_1, q_2, \cdots)$ $q_1 = \begin{bmatrix} 150 & 150 \\ 150 & 150 \end{bmatrix}$ $q_2 = q_3 = \begin{bmatrix} 50 & 50 \\ 50 & 50 \end{bmatrix}$ $q_i = \begin{bmatrix} 0.2 & 0.2 \\ 0.2 & 0.2 \end{bmatrix}, \ i = 3, 4, \cdots 10$	Process noise covariance Q_2	$Q_e = 150 \times \begin{bmatrix} 1 & & \\ & \ddots & \\ & & 1 \end{bmatrix}$
		Measurement noise covariance R_2	$R_e = \begin{bmatrix} 0.05 & 0 \\ 0 & 0.05 \end{bmatrix}$
Control weighting R_k	$R_k = \begin{bmatrix} 0.1 & 0 \\ 0 & 0.1 \end{bmatrix}$	Process noise coupling G_n	$G_n = 0.7 \times \begin{bmatrix} 1 & & \\ & \ddots & \\ & & 1 \end{bmatrix}$
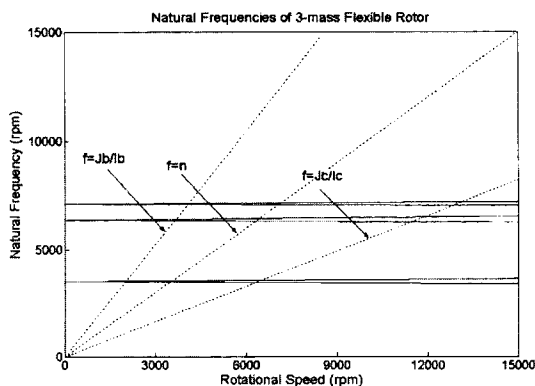
Fig. 9   Campbell diagram of the plant stabilized with PID control

are shown in Fig. 9. Note that there are three critical speeds within operation range (below 10, 000 rpm). The 1st resonance at 3,000 rpm corresponds to the 1st bending of the rotor, and the 2nd and 3rd ones do to those induced by bearing stiffness. The 2nd and 3rd resonance frequencies are slightly different because the flexible coupling breaks the symmetry of the rotor.

The plant stabilized with the PID control is converted into the modal form through bi -orthonormal transformation. Then, balancing of controllability and observability Gramians is performed because of the poor controllability and observability of flexible modes compared to those of rigid ones. The feedback gain of the LQG control is obtained by minimizing the following cost function.

$$J_{LQ} = \frac{1}{2} \int_0^\infty (\chi^T (T_{bal}^{-T} Q_{mod} T_{bal}^{-1}) \chi + u^T R u) \, dt \quad (9)$$

where, $Q_{mod} = diag(q_1, q_2, \cdots)$ $q_i \in R^{2 \times 2}$, and. $\chi = T_{bal} \xi \cdot \chi$ is the balanced state vector, ξ is the modal state vector, and T_{bal} Tbal is the similarity transformation matrix for the balanced realizaion. q_i means the symmetric 2×2 matrix of which diagonal terms contribute to the damping of the ith mode and off-diagonal terms do to the pole movement along the imaginary axis.
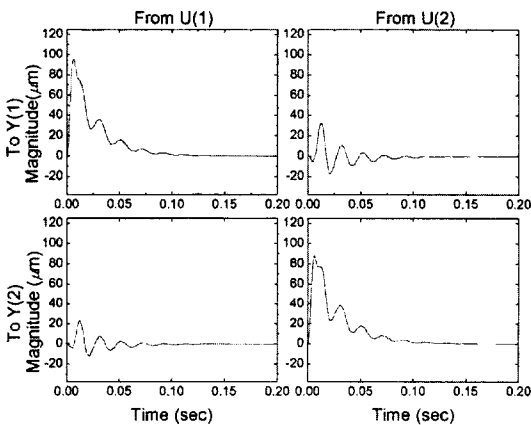
The off-diagonal terms should not be greater than diagonal terms in order to guarnatee the semi-definiteness of weighting function Q_{mod}. The estimator gain matrix is obtained with similar weighting matrices. The order of resulting controller is twenty since we considered ten modes. While an accurate modeling is necessary for reliable application, a low order controller is required for the economic reason. In order to preserve the steady-state gain of the controller, the balanced truncation is adopted and the order of reduced controller is six.
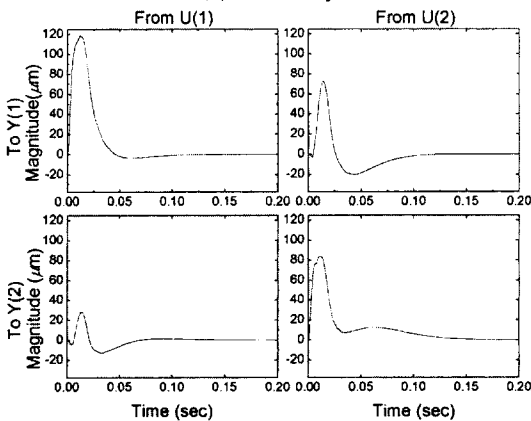
4. Simulation

Prior to implementing the designed controller, simulation with step disturbance is performed in order to see whether the desired performance is satisfied or not. A controller is designed to reduce the peaks of the 1st and 2nd modes because the 2nd and 3rd resonance frequencies are almost identical. The parameters for the LQG control are shown in Table 2. The 1st mode is three times more weighted than 2nd and 3rd ones since the 1st resonance frequency has bigger vibration amplitude than 2nd and 3rd ones. Parameters related to

Kalman filter are chosen so that the poles of Kalman filter are far enough from those of LQ regulator. In addition, covariance matrices are chosen to have equal diagonal values since there is no need to focus on a certain resonance.

The simulation results with step disturbance of 20 N at the plant input are given in Fig. 10. While the 1st resonance frequency means the low frequency vibration in the step response, the 2nd and 3rd do the high frequency vibration. The distortion of the first peak in case of the uncontrolled PID plant means the vibration induced by the 2nd and 3rd resonance frequencies, as shown in Fig. 10(a). The responses to the step disturbance at the plant input go to zero due to the integral action of PID controller. Comparing

Fig. 10(a) and 10(b), we can see that vibrations of the 2nd and 3rd resonance frequencies are almost suppressed as well as the 1st resonance has enough damping after inserting the parallel LQG controller. However, the effect of vibration suppression at several resonance frequencies resulted in a small increase in the peak value of step disturbance, which means the static stiffness decreases a little bit.

5. Experimental Result

Experimental setup is constructed by modifying the RK4 rotor kit (Bently Nevada, 2000) as shown in Fig. 11. Main modifications are for the AMB rotors and units. Experiment setup consists of a flexible shaft with radius of 5 mm and length of 600 mm, one mid-span disk, two AMB units, a flexible coupling, a speed-controlled DC servo-motor. The AMB unit has built-in cylindrical capacitive sensor, which can accurately measure the motion of the geometric center of a rotor (Ahn et al., 2000). The digital controller is implemented with TMS320C44 DSP controller and 8 channel AD/DA. The operation range of the DC motor is up to 10,000 rpm, and the sampling frequency of DSP is 0.1 msec.

The unbalance response of the AMB flexible rotor is obtained by LabVIEW based monitoring system as shown in Fig. 12. This system records and visualizes the unbalance response according to the rotating speed as well as the orbit shape of the rotor in positions of three locations: two AMB rotors and midspan unbalance disk.

(a) PID only

(b) Using parallel LQG controller

Fig. 10 Simulation with step disturbance at the plant input
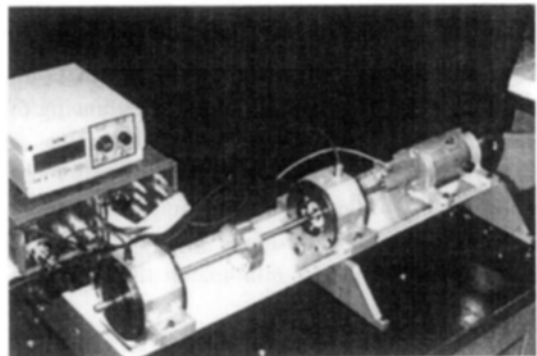
Fig. 11 Experimental setup

The unbalance response for the rotor stabilized with a PID control is shown in Fig. 13. Mass 1 and mass 3 refer to unbalance response at the AMB rotors, and mass 2 indicates the unbalance response at the midspan disk. We can see that there are the two resonance peaks in Fig. 13 because 2nd resonance is almost the same as the 3rd one, as expected in Fig. 9. In addition, the 1st resonance due to the bending mode of the rotor is greater than the second and the third one that are induced by the AMB.

Two LQG controllers are used in order to investigate the effect of the modal weighting. The first controller is designed with weighting the 1st resonance frequency only and the second one is designed with weighting both the 1st and the 2nd resonance frequencies. Unbalance response with
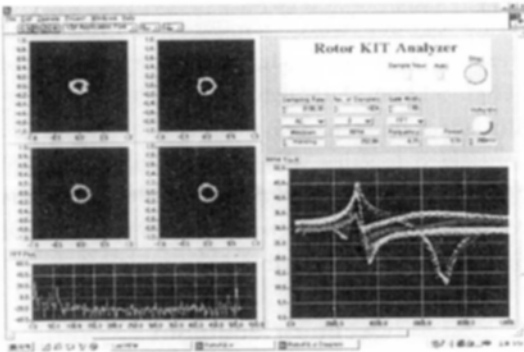
the first controller is shown in Fig. 14, and that with the second one is shown in Fig. 15. Unbalance response is represented in μm by the log magnitude of the orbit radius of each mass. Since we are mainly interested in the unbalance response at the resonant modes, unbalance responses of all masses at a low speed (900 rpm), 1st and 2nd resonance frequencies are shown in Table 3. Figure 14 illustrates that the first bending mode can be fully suppressed with the first controller. Quantitatively, the unbalance response at the 1st resonance peak reduces to the magnitude of less than 10% of that of the original PID controller for all masses. But at the same time, we can notice
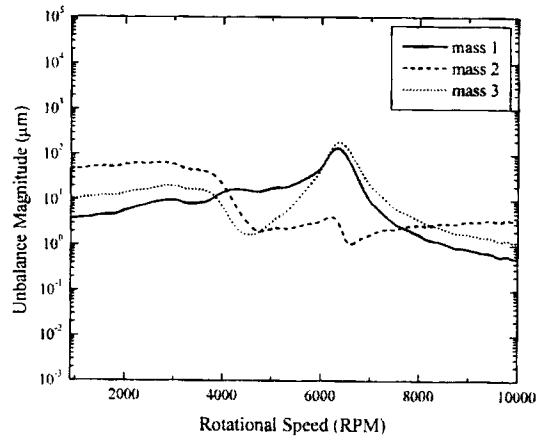

Fig. 12   LabVIEW based monitoring system

Fig. 14   Unbalance response with the weighting of the 1st resonance frequency

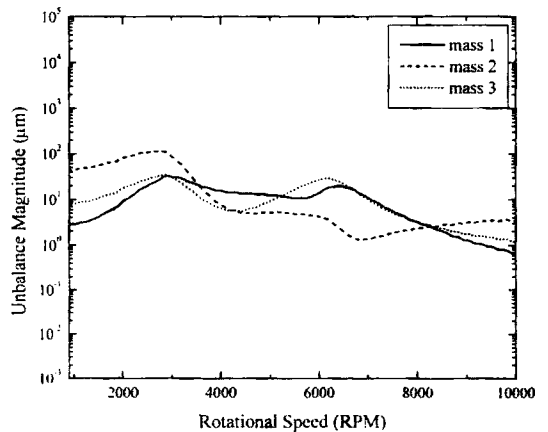Fig. 13   Unbalance response of the plant stabilized with PID control

Fig. 15   Unbalance response with the weighting of both the 1st and 2nd resonance frequencies

Table 3 Magnitude of unbalance responses at the resonant modes and low speed

Controller	Modal Weighting	Magnitude of Unbalance Response (μm)								
		Mass 1			Mass 2			Mass 3		
		Low speed	1st mode	2nd mode	Low speed	1st mode	2nd mode	Low speed	1st mode	2nd mode
PID only	No weighting	1	230	59	30	741	7	3	232	78
PID with LQG 1	1st mode only	4	10	139	48	66	4	11	21	187
PID with LQG 2	1st and 2nd mode	3	32	20	44	112	4	8	34	29

that the minimization of the 1st resonance peak resulted in a little increase of the displacement at low speed and the 2nd resonance peak, which indicates that we cannot fully decouple the modal weighting at each mode.

Figure 15 shows the result of the second controller that is designed with weighting both the 1st and the 2nd resonance frequencies. We can see that both resonance peaks are considerably suppressed, which makes the rotor operate smoothly up to 10,000 rpm without any serious vibration problem. From Table 3, we can notice that the unbalance responses at the 1st and the 2nd resonance frequencies reduce to the magnitude of less than 15% and 35% of those of the PID controller respectively. It also agrees well with the practical aspect of this flexible rotor system that greater resonance suppression is achieved in the midspan disk (mass 2) than the other masses. However, the full suppression of cannot the 1st resonance frequency can be achieved as in the first controller. This suggests again that the modal weighting affects other modes if several modes are considered together. In addition, the responses at very low frequency range grow compared to those with PID control. This means that we lose static stiffness a little, which agree well with the simulation results as shown Fig. 10.

6. Conclusion

Simple procedural steps for system modeling and controller design of the flexible rotor AMB system are proposed in this paper. Based on the

measurement of the open-loop FRF of the system, an accurate model of the AMB flexible rotor is obtained. With this validated model, a parallel LQG controller with modal weighting is designed to reduce the resonance of the system stabilized with a PID control. Simulation and experimental result of unbalance response confirmed the effectiveness of the model validation and control design scheme. Although weighted modes mutually affect other modes when several modes are considered together, the levels of vibration suppression in the experimental results made the rotor operate smoothly within 10,000 rpm without being affected by the vibration problems.

Acknowledgment

References

Ahn, H. J., Jeon, S. and Han, D. C., 2000, "Error Analysis of the Cylindrical Capacitive Sensor for Active Magnetic Bearing Spindles," *J. of Dynamics Systems, Measurement, and Control, Trans. of ASME*, Vol. 122, pp. 102~107.

Ahn, H. J., 2001, "A Study on System Identification and Vibration Control of the AMB Spindle for High Speed Precision Machining Using

Cylindrical Capacitive Sensors," Ph. D. Thesis, Seoul National University, Korea.

Gahler, C. and Mohler, M., 1996, "Multivariable Identification of Active Magnetic Bearing Systems," *5th Int. Symposium on Magnetic Bearings*, Kanazawa, Japan, pp. 7~12.

Ha, Y. H. and Lee, C. W., 1997, "In-situ Modal Testing and Parameter Identification of Active Magnetic Bearing System by Magnetic Force Measurement and the Use of Directional Frequency response functions," *Transactions of KSME A.*, 21(7), pp. 1156~1165.

Kim, S. J. and Lee, C. W., 1998, "On-line Identification of Position and Current Stiffnesses in Active Magnetic Bearing System Equipped with Built-in Force Transducers by LMS Algorithm," *Transactions of KSME A.*, 22(12), pp. 2261~2268.

Lee, C. W. and Kim, J. S., 1992, "Modal Testing and Suboptimal Vibration Control of Flexible Rotor Bearing System by Using a Magnetic Bearing," *J. Dynamic Systems, Measurement and Control*, Vol. 114, pp. 244~252.

Lewis, F., 1992, Applied Optimal Control & Estimation, Prentice-Hall International, Inc.

Nonami, K., 1985, "Vibration Control of Rotor Shaft Systems by Active Control Bearings," ASME *Design Engineering Division Conf.*, Cincinnati, Ohio.

Nonami, K. and Ito, T., 1994, "μ-Synthesis of

Flexible Rotor of Magnetic Bearing System," *4th Int. Symposium on Magnetic Bearings*, Zürich, Switzerland, pp. 73~78.

Okada, Y., Hayashi, H., Saitoh, T. and Shinoda, Y., 1997, "Vibration Control of Flexible Rotor Supported by Magnetic Bearing," *Asia-Pacific Vibration Conference '97*, Kyongju, Korea, pp. 991~996.

Pintelon, R., Guillaume, P., Vandersteen, G. and Rolain, Y., 1998, "Analyses, Development and Applications of TLS Algorithms in Frequency Domain System Identification," SIAM *J. Matrix Anal. Appl.* .

RODAP (ROtating machine Design and Analysis Program), D&M Technology Co., Korea.

RK4 Rotor kit, Bently-Nevada Co., USA.

Salm, J. R., 1988, "Active Electromagnetic Suspension of an Elastic Rotor : Modeling, Control, and Experimental Results," ASME *Journal of Vibration, Acoustics, Stress, and Reliability in Design*, Vol. 110, October, pp. 493~500.

Schönhoff, U., Luo, J., Li, G., Hilton, E., Nordmann, R. and Allaire, P., 2000, "Implementation Results of μ-Synthesis Control for an Energy Storage Flywheel Test Rig," *7th Int. Symposium on Magnetic Bearings*, Zürich, Switzerland, pp. 317~322.

Schweitzer, G., Bleuler, H. and Traxler, A., 1994, *Active Magnetic Bearings*, Hochschulverlag AG de ETH Zürich, Switzerland.